Eur. Phys. J. D **14**, 97–103 (2001)

THE EUROPEAN PHYSICAL JOURNAL D

EDP Sciences
© Società Italiana di Fisica
Springer-Verlag 2001

Design study of 3-D tomography diagnostics for spherical tokamaks

A.L. Balandin[a], Y. Ono[b], and T. Tawara

High-Temperature Plasma Center, University of Tokyo, 2–11–16 Yayoi, Bunkyo–ku, Tokyo 113–8656, Japan

Received 17 August 2000 and Received in final form 16 November 2000

Abstract. A novel three-dimensional (3-D) tomography software has been developed for spherical tokamak (ST) plasmas with thin central coils. It enables us to measure whole 3-D annular profiles of ST plasma emissivity (line spectrum etc.) using limited number of detectors located on a sphere outside of its separatrix. The numbers and positions of detectors have been optimized for STs that contain low-n toroidal modes from $n = 1$ to 5. Mathematical method allowing for the removal of the thin central coil from the region of reconstruction and to reconstruct STs with single and double axes are also discussed. The shadow effect of center coil region was found to limit the reconstruction accuracy, indicating that the low-aspect ratio torus (ST) is essential to this new 3-D tomography diagnostics.

PACS. 07.05.Tp Computer modeling and simulation – 02.60.Cb Numerical simulation; solution of equations – 52.70.Kz Optical (ultraviolet, visible, infrared) measurements

1 Introduction

Tomography diagnostics are powerful tool for fusion plasma diagnostic using multiple line-integrated signals, such as soft X-ray, plasma emission and interferometric diagnostics. Spherical tokamaks has a unique possibility to extend those tomography diagnostics from 2-D to 3-D. Its central coil region is too narrow to install detectors for the conventional 2-D tomography of poloidal plane but its compact spherical geometry has a good potential to install those all around its spherical separatrix, extending the conventional 2-D tomography into 3-D. However, central conductor is an opaque obstruction for emission radiation and projections in this case will have data-missing parts. From the mathematical point of view, this is a problem with incomplete data set, which tends to be severely ill-posed, suggesting that the reconstructed image in this case may be degraded fatally [2]. Three dimensional algorithm based on the maximum entropy principle was adopted for tomographic reconstruction from projections with data-missing parts. This method according to Jaynes [1] gives "... the least biased estimate possible on the given information; *i.e.*, it is maximally noncommittal with regard to missing information". The main idea of modification comes from Gerchberg [3], Papoulis [4] algorithm and applied to the tomography problems in [5]. This algorithm based on the idea of "artificial" translucence of an opaque medium, which means that the lost information concerning the data-missing part of one viewing position can be recovered by measured data from the other directions. Iterative modifications using a prior information about outline and position of opaque obstruction permit to recovery surrounding part of the opaque obstruction. Other methods related to the problem with incomplete set of measurements are considered in [6–8].

This paper described a new method of 3-D tomography reconstruction for spherical tokamak diagnostics – mainly a visible light tomography using plasma line spectrum. The scheme of measurements is given in Figure 1. The spherical tokamak device TS-4 was used to develop the whole system but can be easily extend to any spherical tokamak experiment. The TS-4 device can produce one or two spherical tokamaks with major radius of 0.5 m and aspect ratio of 1.2–1.9 inside its cylindrical vacuum with length of 2 m and diameter of 1.8 m. Its spectrum line emission of various impurity species are measured by detectors located inside and outside of the vacuum vessel. The 3-D emission profile obtained will be useful to monitor ST plasma shape, for example during its internal reconnection event (IRE) and will be used to measure 3-D flow and ion temperature in future based on extension of the present system. In this paper the results of computer simulation has been made for several toroidal type models of emissivity distribution to optimize the basic design concept such as the number of detectors and their positioning. The models used were related to the real (experimental) emissivity distribution and represents toroids perturbed by toroidal modes up to $n = 5$. We examine how the accuracy of reconstruction is affected

[a] e-mail: balandin@katsurai.t.u-tokyo.ac.jp (on leave from the Institute of System Dynamics and Control Theory, Lermontov str. 134, 664033, Irkutsk, Russia).

[b] e-mail: ono@katsurai.t.u-tokyo.ac.jp

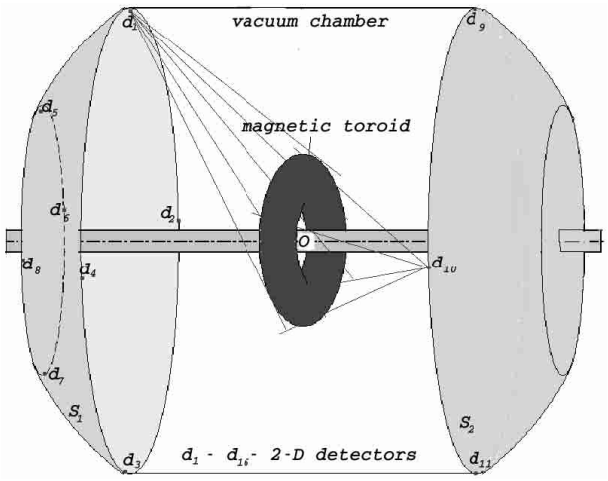

Fig. 1. Scheme of measurements for 3-D tomography of plasma diagnostic.

by the major global instabilities of ST and spheromak. The major instability expected has $m/n = 1/1$ mode and $m/n = 1/2, 1/3$ ones in the present spheromak and ST experiments. The $m/n = 1/1$ mode causes the major/minor disruption of ST and $1/2, 1/3$ modes are essential to the dynamics of spheromaks. The influence of the central conductor on the emissivity distribution as well as the quality of reconstruction against the number of registered projections was studied.

2 Method of inversion

To start, let $\varepsilon = \varepsilon(\mathbf{x})$ is the three-dimensional object to be reconstructed. It is assumed that the support of ε is a ball with unit radius. The measurable data for cone beam geometry are assume to be defined by the formula (3) below. We shall use three systems of reference: two Cartesian systems $\mathbf{x} = (x, y, z)$ and $\mathbf{x}_j = (x_j, y_j, z_j)$, laboratory one and rotating system of projections registration, respectively and cone coordinates $\mathbf{u}_j = (u_j, v_j, w_j)$ related to the $\mathbf{x}_j$ system [9]. The transformation of coordinate system $\mathbf{x} = (x, y, z)$ to $\mathbf{x}_j = (x_j, y_j, z_j)$ is performed by the rotation matrix $R_j(\alpha, \beta)$

$$\mathbf{x}_j = R_j \mathbf{x}. \tag{1}$$

The expression for the matrix R_j in terms of the Euler angles α $(0 \le \alpha < 2\pi)$, β $(0 \le \beta \le \pi)$ is given by

$$R_j(\alpha, \beta) = \begin{pmatrix} \cos\beta\cos\alpha & \cos\beta\sin\alpha & -\sin\beta \\ -\sin\alpha & \cos\alpha & 0 \\ \sin\beta\cos\alpha & \sin\beta\sin\alpha & \cos\beta \end{pmatrix},$$

where angle α is specified by the rotation about the z-axis and β is specified by the rotation about the new y_j-axis. The cone coordinate (u_j, v_j, w_j) with the vertex at $z_j = -d_j$ are written in the rotated system of coordinates (x_j, y_j, z_j) by the following transformation

$$u_j = \frac{x_j}{1 + z_j/d_j}, \qquad x_j = u_j(1 + w_j/d_j), \tag{2a}$$

$$v_j = \frac{y_j}{1 + z_j/d_j}, \qquad y_j = v_j(1 + w_j/d_j), \tag{2b}$$

$$w_j = z_j, \qquad z_j = w_j. \tag{2c}$$

For the simplicity of notations the following functional dependences for direct and inverse transformations are used for $j = 1, 2, ..., J$

$$\begin{aligned} u_j &= U_j(x_j, y_j, z_j), & x_j &= X_j(u_j, v_j, w_j), \\ v_j &= V_j(x_j, y_j, z_j), & y_j &= Y_j(u_j, v_j, w_j), \\ w_j &= W_j(x_j, y_j, z_j), & z_j &= Z_j(u_j, v_j, w_j). \end{aligned}$$

Without loss of generality we can assume that the measured data of the jth cone beam is known on the (x_j, y_j)-plane. The relation between the unknown source function $\varepsilon(\mathbf{x})$ and the projection functions $I_j(u, v)$ measured on the (x_j, y_j)-plane is

$$\begin{aligned} I_j(u, v) &= \int_{R^2} \mathrm{d}\mathbf{x}\, \varepsilon(\mathbf{x})\, \delta\big(u - U_j(\mathbf{x})\big)\delta\big(v - V_j(\mathbf{x})\big) \\ &= \int_{l_j} \mathrm{d}w \left|\frac{\partial(x, y, z)}{\partial(u, v, w)}\right| \varepsilon\big(x_j, y_j, z_j\big), \end{aligned} \tag{3}$$

where the Jacobian matrix, $\mathcal{J}$, of the transformation is simply calculated using (1, 2) and equals

$$\mathcal{J} = \frac{\partial(x, y, z)}{\partial(u, v, w)} = (1 + w/d_j)^2.$$

Using Lagrange approach [10] we should maximize the following Lagrange functional:

$$L(\varepsilon, \boldsymbol{\Lambda}) = \eta(\varepsilon) - \sum_{j=1}^{J} \int \mathrm{d}u\mathrm{d}v\, \Lambda_j(u, v)\tilde{I}_j(u, v), \tag{4}$$

$$\tilde{I}_j(u, v) = I_j(u, v) - \int \mathrm{d}w\, |\mathcal{J}| \varepsilon(x_j, y_j, z_j)$$

where integration is executed over the definition region of (u, v, w), $\boldsymbol{\Lambda} = (\Lambda_1, \Lambda_2, ..., \Lambda_J)$ is Lagrange multiplier and $\eta(\varepsilon)$ is the entropy functional is defined as follows

$$\eta(\varepsilon) = -\int_{\mathrm{D}} \mathrm{d}\mathbf{x}\, \varepsilon(\mathbf{x}) \ln(\varepsilon(\mathbf{x})V), \tag{5}$$

V is some normalization constant, D is the region of reconstruction.

A change of variables takes the second integral in (4) to the form

$$\int_{\mathrm{D}} \mathrm{d}\mathbf{u}|\mathcal{J}|\Lambda_j(u, v)\varepsilon(\mathbf{u}) = \int_{\mathrm{D}} \mathrm{d}\mathbf{x}\, \varepsilon(\mathbf{x})\Lambda_j\big(U_j, V_j\big). \tag{6}$$

Taking the variation of (4) with respect to the function ε and equating it to zero, we obtain

$$\varepsilon(\mathbf{x}) = \frac{1}{V}\prod_{l=1}^{J} H_l\big(U_l(\mathbf{x}), V_l(\mathbf{x})\big), \tag{7}$$

where $H_l(U_l, V_l) \equiv \exp(\Lambda_l(U_l, V_l) - 1/J)$. The unknown functions $H_l(U_l, V_l)$ can be evaluated *via* the substitution of the equation (7) into the constraints (3):

$$I_j(u,v) = \frac{1}{V}\int\limits_{l_j} \mathrm{d}w\,|\mathcal{J}| \prod_{l=1}^{J} H_l\big(U_l, V_l\big). \tag{8}$$

The following equations for the functions H_j is obtained:

$$I_j(u,v) = \frac{1}{V} H_j(u,v) \int\limits_{-\infty}^{\infty} \mathrm{d}w\,|\mathcal{J}| \prod_{l\neq j}^{J} H_l\big(U_{lj}, V_{lj}\big), \tag{9}$$

where $U_{lj} \equiv U_l(x_j, y_j, z_j)$, $V_{lj} \equiv V_l(x_j, y_j, z_j)$. This leads to the following iterative scheme:

$$H_j^{i+1}(u,v) = \frac{I_j(u,v)V}{\displaystyle\int\limits_{l_j} \mathrm{d}w\,\big|1 + w/d_j\,\big|^2 \prod_{l\neq j}^{J} H_l\big(U_{lj}, V_{lj}\big)} \tag{10a}$$

$$\text{for} \quad j = i \pmod J + 1;$$

$$H_j^{i+1}(u,v) = H_j^i(u,v), \tag{10b}$$

$$\text{for} \quad j \neq i \pmod J + 1;$$

$$H_j^0(u,v) = \begin{cases} 1, & \text{if } I_j(u,v) \neq 0, \\ 0, & \text{if } I_j(u,v) = 0. \end{cases} \tag{10c}$$

This describes the main part of the inversion algorithms. The idea of "artificial" translucence is realized in the following way. At first, the missing data at the projections are recovered by any method of interpolation. The above inversion algorithm is applied to get some estimation of emissivity distribution. After that the projection data are calculated numerically and is kept only shadowing part of the projections, any other values are taken from the experimental data. On this step any a prior information can be added, for instance positiveness. This step is fundamental for Fourier reconstruction method or filtering back projection one.

3 Computer simulation

This section describes the results of computer simulation for demonstration of the algorithm. Several models closely related to the real emissivity distribution in plasma device, given as toroids perturbed by the following toroidal modes $n = 3, 4, 5$ are considered here. Each toroid of a complex model[1] is defined by the formulas

$$\begin{aligned} x &= \left(\sum_{n=0}^{N} R_n \cos(n\varphi) + r\cos\theta\right)\sin\varphi \\ y &= \left(\sum_{n=0}^{N} R_n \cos(n\varphi) + r\cos\theta\right)\cos\varphi \\ z &= r\sin\theta, \end{aligned} \tag{11}$$

where R_0 is the major axis, θ and φ are the poloidal and toroidal angles, respectively. In the case of $n = 0$ the circle with radius R_0 is called the minor axis. The parameter r is called the minor radius and measures the distance from the minor axis. The distribution of emissivity is taken as exponential function $A_j \exp(-a_j r^2)$, over the minor radius r in a toroid, $a_j > 1$ is a positive constant, j is a toroid number in a complex model. All reconstructions was performed with the data spoiled by some artificial noise. The noise level was taken as 2.5% of maximum level of measured data (projections). The discrepancy between exact and reconstructed models is a relative discrete analogue of Hilbert norm and has the following form

$$\Delta^2 = \frac{\displaystyle\sum_{i=0}^{M} (\varepsilon_i - \tilde{\varepsilon}_i)^2}{\displaystyle\sum_{i=0}^{M} \varepsilon_i^2}, \tag{12}$$

where summation is performed over all grid points of 3-D reconstruction region, ε_i and $\tilde{\varepsilon}_i$ are the value of the exact model and its estimation at the ith point of the grid. Three dimensional images of exact and reconstructed toroids for different toroidal mode n are given in Figures 2–4. In a numerical experiments it was used total number 16 of 2-D projections, each of them contains 21×21 number of ray-sums. The detectors located on the four slices of spherical surfaces S_1, S_2, symmetrically disposed over device's middle plane. In general the detectors can be set up at any points of the surfaces S_1 and S_2 (important only to keep the distance between detectors and point O in Fig. 1). The radius of shadowing obstruction is $\rho = 0.14R$, which corresponds to the real size in our device, where R is a radius of the vacuum chamber. For shadow effect observing fat toroid is chosen and radius of opaque obstruction is enlarged up to $\rho = 0.3R$. The fat toroid without opaque obstacle and its reconstruction is given in Figure 4. The same one with a presence of opaque obstacle and result of reconstruction are given in Figure 9. An axis z of the coordinate system is oriented at an angle of 50° to the page normal. For the internal emissivity distribution investigation the fat toroids, exact end reconstructed, was dissected by the planes $y{-}z$ (Fig. 5) and $x{-}y$ (Fig. 7). One-dimensional sections of $y{-}z$ and $x{-}y$ planes are shown in Figures 6 and 8, respectively. The exponential emissivity distribution along minor radius r can be observed. An error of reconstruction (in per cent) for different toroidal

[1] The model is a complex one if it contains more then one toroid.

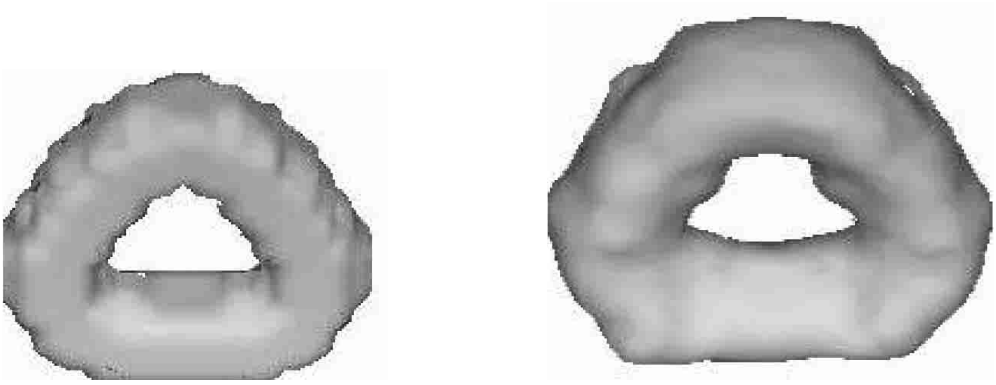

(a) (b)

Fig. 2. (a) Perturbed toroid with aspect ratio $A = 3.5$ by the toroidal mode $n = 3$ and (b) its reconstruction. Relative error of reconstruction is 25.3%.

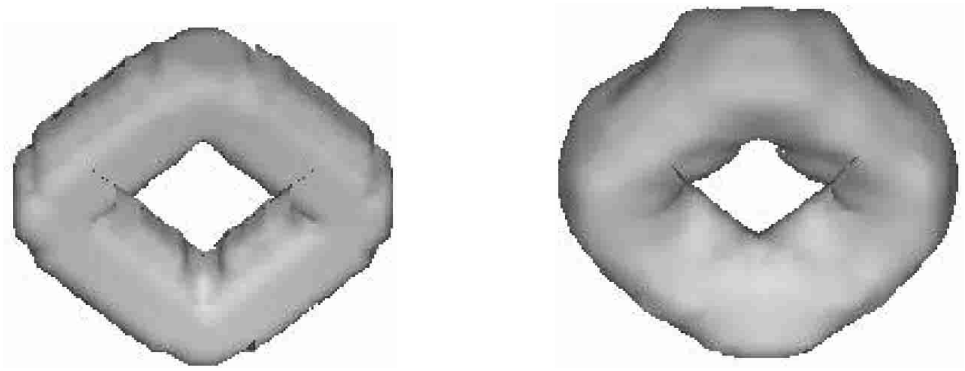

(a) (b)

Fig. 3. (a) Perturbed toroid with aspect ratio $A = 3.5$ by the toroidal mode $n = 4$ and (b) its reconstruction. Relative error of reconstruction is 23.8%.

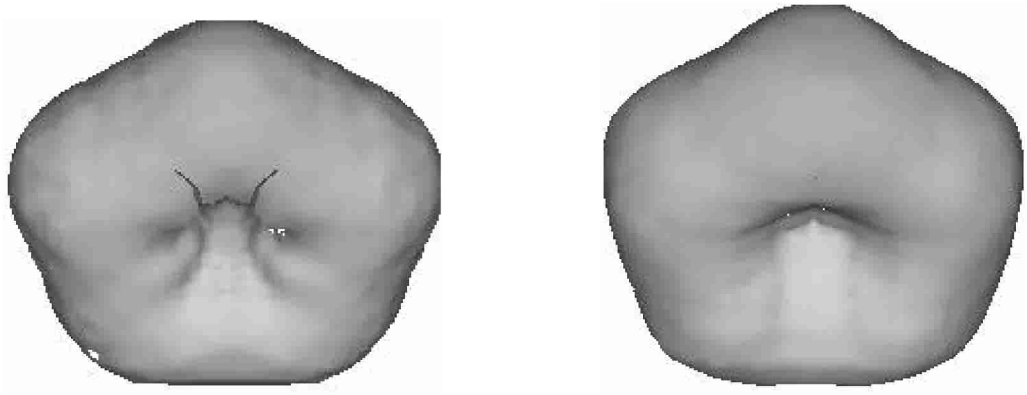

(a) (b)

Fig. 4. (a) Fat perturbed by the toroidal mode $n = 5$ toroid with aspect ratio $A = 1.0$ (without opaque obstruction) and (b) its reconstruction. Relative error of reconstruction is 3.35%.

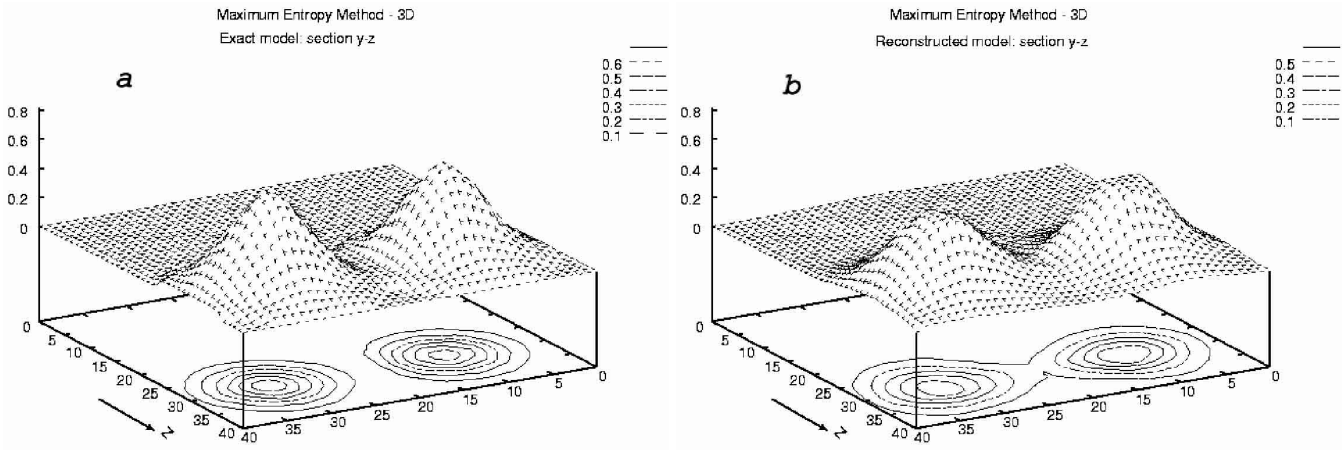

Fig. 5. (a) Sections of exact and (b) reconstructed fat toroids mode $n = 5$ by the plane $y{-}z$.

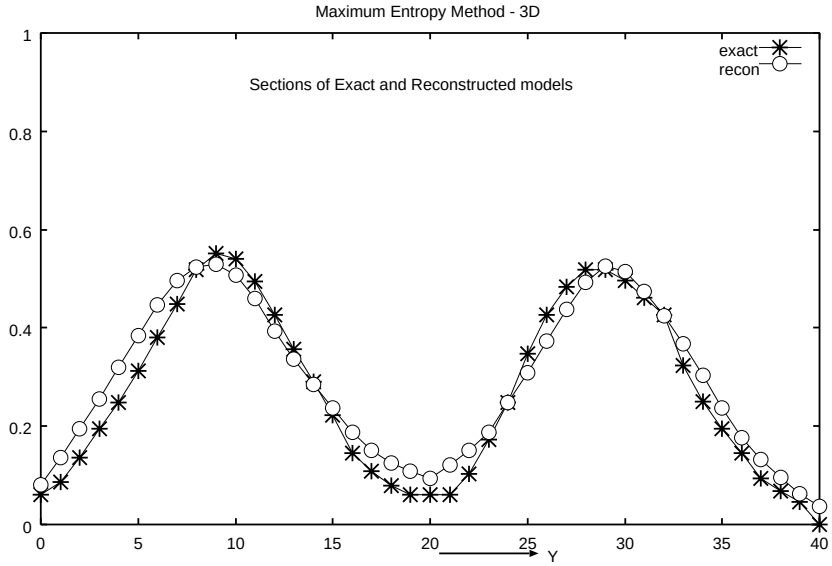

Fig. 6. Section of the plane $y{-}z$ by the line $z = 33$ of exact (—∗—) and reconstructed (—○—) models.

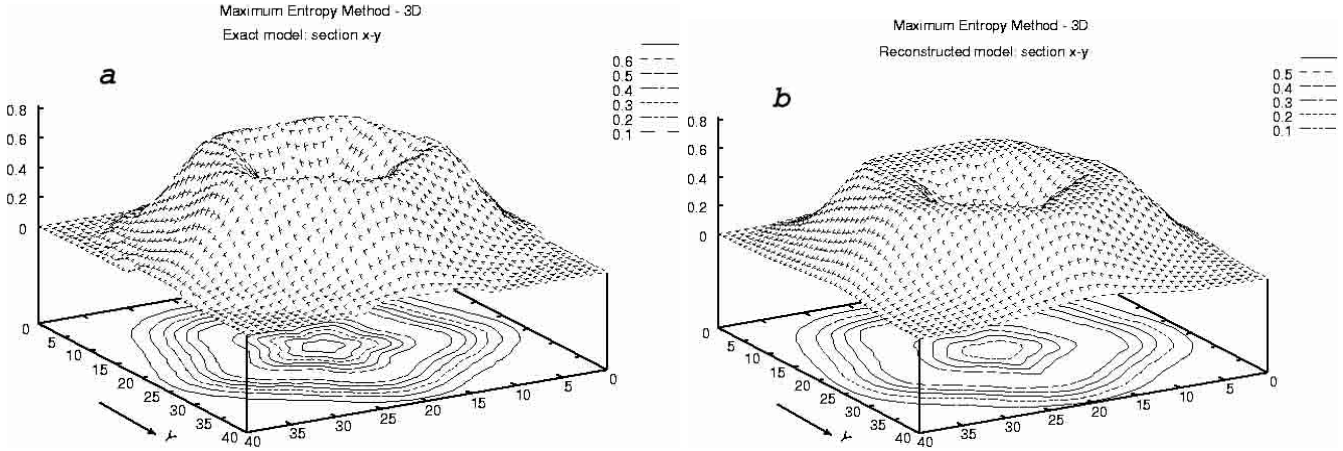

Fig. 7. (a) Sections of exact and (b) reconstructed fat toroids mode $n = 5$ by the plane $x{-}y$.

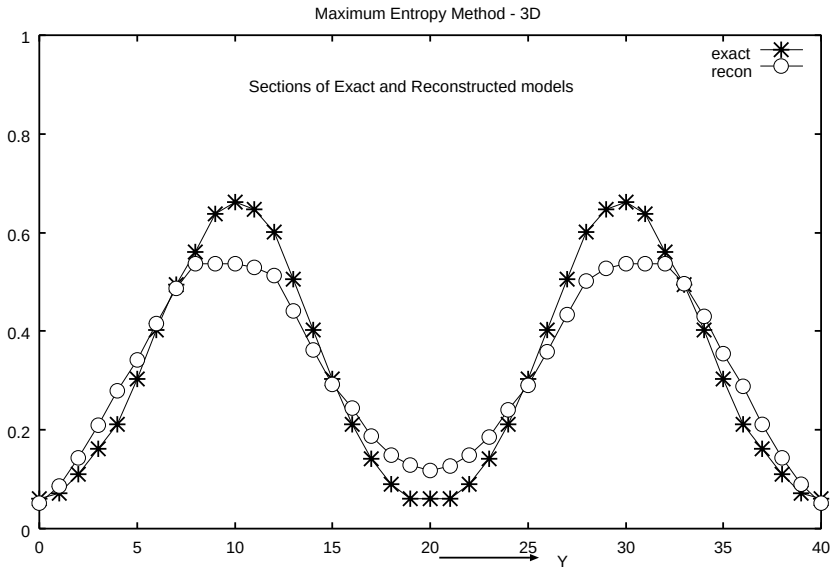

Fig. 8. Section of the plane $x-y$ by the line $y = 23$ of exact (—∗—) and reconstructed (—○—) models.

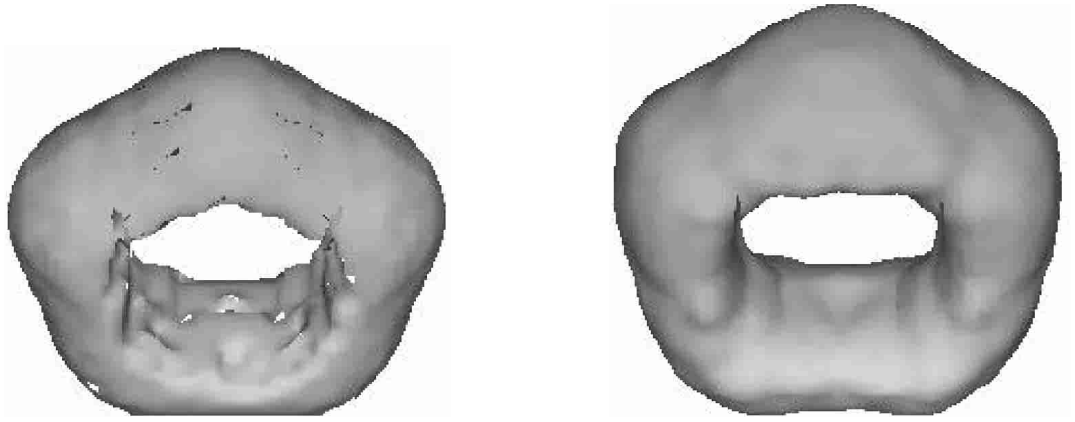

(a) (b)

Fig. 9. (a) Fat perturbed toroid by the toroidal mode $n = 5$ with presence of opaque obstruction and (b) its reconstruction. Relative error of reconstruction is 20.2%.

modes $n = 1, 2, 3$ against summary number of projections is shown in Figure 10. As is apparent from Figure 11 the error of reconstruction essentially depends on the total number of projections and position of the detectors. It was used 24 total number of projections (three slices on each spherical surface S_1 and S_2) for the reconstruction of mode $n = 3$ in this experiment. The difference between curves (—∗—) and (—○—) is caused by different positions of detector's slices on the S_1 and S_2 surfaces. The result indicates that computer modeling is an essential step previously to diagnostic system design. Three curves of a reconstruction error for mode $n = 1$ with different aspect rations A is plotted in Figures 12a and 12b. Figure 12a shows the error of reconstruction against the aspect ratio A. The radius of an opaque obstruction is equal to $\rho = r(A - 1)$. The curves of the reconstruction errors without (—∗—) and with constant (—○—) opaque obstruction radius $\rho = 0.14R$, respectively are shown in Figure 12b. The difference between those two curves means an influence of central conductor shadow effect on the quality of reconstruction for different aspect ratio toroids. In the vicinity of $A = 2$ minor radius becomes comparable with the grid step of projection registration and shadow effect shrink to a nullity.

4 Conclusion

We have developed (by numerical modeling) a new 3-D tomographical scheme suitable for spherical torus plasmas diagnostics such as visible light/soft X-ray tomographies. Our maximum-entropy scheme was examined to reconstruct whole annular plasma shape with low-n toroidal mode from $n = 1$ to 5, if we set sufficient number of detectors around the ST. Its reconstruction accuracy is

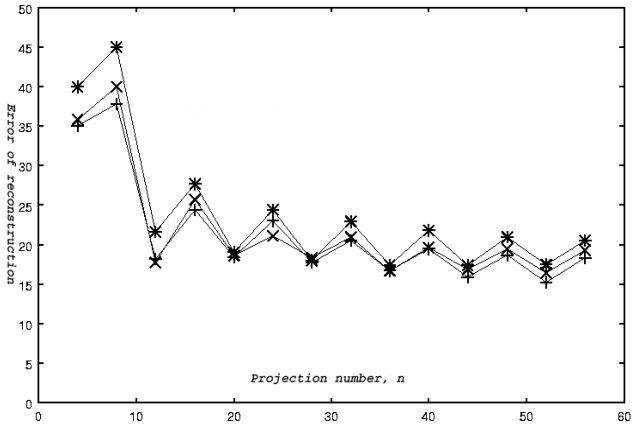

Fig. 10. The reconstruction error (in per cent) against projections number for different toroidal modes: $n = 1$ (—+—), $n = 2$ (—×—), $n = 3$ (—∗—).

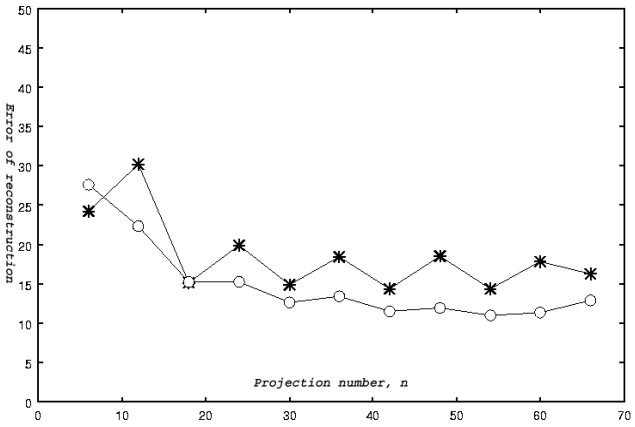

Fig. 11. Another geometry of observation: six detector's slices on S_1 and S_2 surfaces is used. The error of reconstruction (in per cent) on the total number of projections for the mode $n = 3$ is shown. The dissimilarity between (—∗—) and (—○—) curves is at difference detector's slices position.

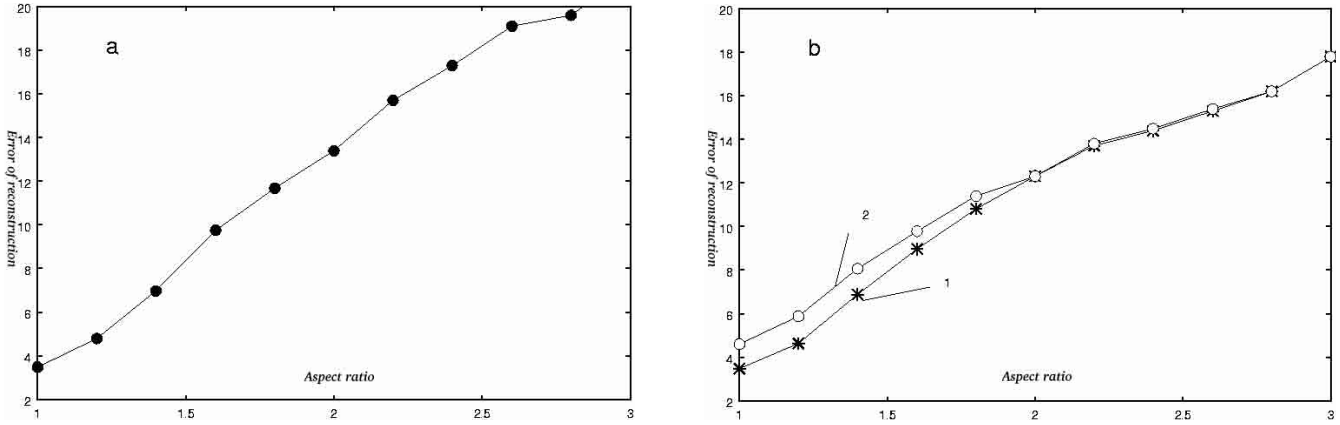

Fig. 12. Dependence of the reconstruction error (in per cent) of toroidal mode $n = 1$ on the aspect ratio A; (a) with opaque obstruction radius of $\rho = r(A - 1)$, (b) without (—∗—) and with constant (—○—) opaque obstruction radius of $\rho = 0.14R$, respectively.

determined by shadow effect of central coil, by the numbers of detectors and also by the number of viewing lines. Detailed study of reconstruction errors revealed its optimal scheme; positions and numbers of detectors. The most cost-effective number of detector was observed to be 8–16, based on a minimum point of reconstruction error multiplied by detector numbers. Under the presence of 2.5% noise the reconstruction error of the optimal case was about 17%, so this method is quite attractive for a real ST tomography diagnostic system.

The first author would like to express his gratitude to the staff of High-Temperature Plasma Center, University of Tokyo, for their great hospitality.

References

1. E.T. Jaynes, Phys. Rev. **106**, 620 (1957).
2. F. Natterer, *The Mathematics of Computerized Tomography* (John Wiley & Sons Ltd and B.G. Teubner, Stuttgart, 1986).
3. R.W. Gerchberg, Opt. Acta **21**, 709 (1974).
4. A.A. Papoulis, IEEE Trans. Circuits Syst. **22**, 735 (1975).
5. A.L. Balandin, V.V. Pickalov, N.G. Preobrazhensky, in *Proceedings of the IV All-Union Symposium on Computerized Tomography*, 1989, edited by M.M. Lavrentiev, Novosibirsk, p. 68 (in Russian).
6. B.E. Oppenheim, IEEE Trans. Nucl. Sci. **21**, 72 (1974).
7. R.M. Lewitt, R.H. Bates, Optik **50**, 189 (1978).
8. R.M. Lewitt, R.H. Bates, Optik **50**, 269 (1978).
9. G. Minerbo, Comput. Biol. Med. **9**, 29 (1979).
10. M.S. Bazaraa, C.M. Shetty, *Foundations of optimization* (Springer-Verlag, Berlin, New York, 1976).